Inorganica Chimica Acta 430 (2015) 216–224

Contents lists available at ScienceDirect

Inorganica Chimica Acta

journal homepage: www.elsevier.com/locate/ica

Association of late transition metal complexes with ethyl 2-(2-(4-chlorophenylcarbamothioyl)hydrazono)propanoate: Design, synthesis and *in vitro* anticancer studies

Aishakhanam H. Pathan [a], Asha K. Ramesh [b], Raghavendra P. Bakale [a], Ganesh N. Naik [a], H.G. Rohit Kumar [b], Christopher S. Frampton [c], Gopal M. Advi Rao [b], Kalagouda B. Gudasi [a,*]

[a] Department of Chemistry, Karnatak University, Dharwad 580 003, Karnataka, India
[b] Department of Biochemistry, Davangere University, Davangere 577002, Karnataka, India
[c] SAFC Pharmorphix, A Sigma-Aldrich Company, 250 Cambridge Science Park, Milton Road, Cambridge CB4 0WE, UK

ARTICLE INFO

Article history:
Received 15 October 2014
Received in revised form 24 December 2014
Accepted 5 March 2015
Available online 20 March 2015

Keywords:
Ethyl pyruvate
Thiosemicarbazone
Metal complexes
X-ray structure
Apoptosis
Caspase-3 activity

ABSTRACT

A newly synthesized chelating agent ethyl 2-(2-(4-chlorophenylcarbamothioyl)hydrazono)propanoate with SNO donor sites is employed for the synthesis of Co(II), Ni(II), Cu(II) and Zn(II) complexes. Structure of ligand is determined by single crystal X-ray diffraction analysis. Octahedral geometry is assigned to all the complexes based on the physical and spectral data. The copper complex has shown redox responses in the applied voltage range, whereas the ligand and other complexes are electrochemically inactive. The new complexes synthesized have been evaluated for *in vitro* antiproliferative activity against human cancer cells of different origin such as COLO-205 and K-562. Among the compounds tested for their antiproliferative activity, IC_{50} value of copper complex is 15.16 and 8.65 μM for K-562 and COLO-205, respectively. Time dependent significant fall in mitochondrial membrane potential ($\Delta\Psi_m$) without generating reactive oxygen species (ROS) is observed in COLO-205 cells treated with copper complex, whereas its antiproliferative effect mediated by the induction of apoptotic cell death is evidenced by the sub-G_0/G_1 cells accumulation, oligonucleosomal DNA fragmentation, caspase-3 activation and the nuclear condensation. Further results confirmed subsequent apoptosis induction through activation of intrinsic apoptotic pathway.

1. Introduction

Metal based drugs such as organoplatinum compounds are extensively used in cancer chemotherapy [1–3]. The clinical utility of these compounds is limited to a relatively narrow range of tumors (sarcomas, small cell lung cancer, ovarian cancer, lymphomas and germ cell tumors) [4,5], by dose-limiting side effect and acquired resistance due to prolonged administration. To circumvent these problems, much attention has been focused on designing unconventional metallo-organic compounds which greatly facilitate the interaction of the biomolecules in biological systems [6–9]. Recently it is shown that cupredoxin azurin preferentially enter cancer cells rather than normal cells and form complex with the tumor suppressor protein PS3, stabilizing it and increasing its intracellular level, thereby inducing apoptosis via corpus mediated mitochondrial pathway [10].

Thiosemicarbazone of ethyl pyruvate (EP) derivatives have been a subject of interest to researchers of different profiles including pharmacologists and coordination chemists [11–15]. These derivatives have shown promising antitumor activity against various cancer cell lines [16,17]. Their biological activities are explained on the basis of various mechanisms including intercalation properties, inhibition of DNA and RNA, breaking of DNA strands, alteration of cell membrane functions and free radical mediated alkylation [18,19]. Thus, a combination of such a small molecule (EP) with potent cytotoxic thiosemicarbazide pharmacophore may act in an additive or synergistic mode, showing effect on the DNA-binding properties of the parental moiety. Metallo-organic compounds of such derivatives tend to be strongly mutagenic and have shown promising chemotherapeutic activities. Elevated intracellular metal levels in particular copper levels predispose cancerous cells to ionophoric copper sensitivity. Several copper coordinating lipophilic thiosemicarbazone compounds are being investigated as potential anticancer therapeutics [20].

* Corresponding author. Tel.: +91 836 2215286 (O); fax: +91 836 2771275.
E-mail address: kbgudasi@gmail.com (K.B. Gudasi).

http://dx.doi.org/10.1016/j.ica.2015.03.013
0020-1693/

Therefore, in the present work, as a part of our search for new molecules with anticancer activity, we have focused our attention toward the synthesis of ethyl pyruvate derived thiosemicarbazone ligand (E)-ethyl 2-(2-(4-chlorophenylcarbamothioyl)hydrazono)-propanoate and its cobalt (CoL_2), nickel (NiL_2), copper (CuL) and zinc (ZnL_2) complexes. These were characterized thoroughly and systematically tested for their anticancer activity. Among all the complexes tested, copper complex was found to be more active on colon adenocarcinoma. Using varied lines of experimental strategies, it is shown that copper complex induces cell death through apoptotic mode. Thus the present results might open a new insight in the design of a new type of metal based therapeutic agent.

2. Experimental protocols

2.1. Materials and methods

All the reagents are commercially available (Aldrich or Merck) and used as supplied. Solvents were purified and dried according to standard procedures. Thiosemicarbazone was prepared according to the earlier reports with slight modifications [21]. Metal chlorides used were in the hydrated form. Metal content was determined according to the standard methods. Melting points (m.p.) were determined in open capillaries and are uncorrected. The molar conductivity was measured on ELICO-CM-82 Conductivity Bridge. Infrared spectra were recorded in KBr discs in the region 4000–400 cm^{-1} on a Nicolet 170 SX FT-IR spectrophotometer. ^1H and ^{13}C spectra of the ligand were recorded in $(CD_3)_2SO$ on a BRUKER 500 MHz spectrometer. All the compounds were analyzed for Carbon, Hydrogen, Nitrogen and Sulfur by Thermo quest elemental analyzer. Electronic spectra of all the compounds in DMSO were recorded on a UV–Vis spectrophotometer (Varian Cary 50 Bio). Magnetic susceptibilities at room temperature were determined using a Gouy balance with $Hg[Co(SCN)_4]$ as the reference compound and magnetic moments were calculated making the necessary diamagnetic corrections. Thermal analysis of the metal complexes were carried out in nitrogen atmosphere on universal V2.4F TA Instrument keeping final temperature at 1000 °C with a heating rate of 10 °C/min. The cyclic voltammetric experiments were carried out with a three electrode apparatus using a CHI1110A electrochemical analyzer (USA). The EPR spectra of copper complex were recorded on a Varian E-4 X-band spectrometer using TCNE as g-marker.

2.1.1. Preparation of ethyl 2-(2-(4-chlorophenylcarbamothioyl)hydrazono)propanoate (LH)

The ligand (LH) was prepared in two steps. First, 4-(4-chlorophenyl)thiosemicarbazide was obtained and purified by the literature method [22]. It (0.201 g, 1 mmol) was then refluxed with methanolic solution (20 mL) of ethyl pyruvate (0.116 g, 1 mmol) for 2 h. Partial evaporation of the solvent yielded crystals suitable for X-ray single crystal analysis which were filtered off, washed with methanol and dried in vacuum (Scheme 1).

Yield: 86%; mp: 133–135 °C.

$C_{12}H_{14}ClN_3O_2S$: *Anal.* Calc. C, 48.07; H, 4.71; N, 14.02; S, 10.70%. Found: C, 48.10; H, 4.77; N, 13.98; S, 10.73%. IR (cm^{-1}). 3249, Hydrazine NH; 3290, Phenyl NH; 1685, C=O; 1627, C=N. ^1H NMR (DMSO-d_6) ppm: 11.01 (s, 1H, Hydrazine NH), 10.00 (s, 1H, NH phenyl), 4.20–4.23 (m, J = 5, 2H, CH_2), 2.17 (s, 3H, N=C=CH_3), 1.26 (t, J = 5, 3H, CH_3), ^{13}C NMR (DMSO-d_6) δ: 177.71 (C=S), 164.14 (C=O), 140.07 (C=N), 61.25 (CH_2), 14.02 (CH_3).

2.1.2. Preparation of the complexes

To a hot solution of LH (1 mmol) in methanol (20 mL) was slowly added, a hot solution of the metal chlorides Viz: Co(II), Ni(II), Cu(II) and Zn(II) (1 mmol) in methanol (5 mL) and the mixture was stirred at room temperature for 4 h. The precipitates obtained were filtered, washed thoroughly with methanol, then with ether and dried in *vacuo*. Attempts to grow single crystals were unsuccessful. The proposed structures of the complexes are given in Scheme 2.

2.1.2.1. $C_{24}H_{26}Cl_2N_6O_4S_2Zn$ (ZnL_2). Anal. Calc. C, 43.48; H, 3.95; Cl, 10.70; N, 12.68; O, 9.65; S, 9.67; Zn, 9.86%. Found: C, 43.47; H, 3.95; Cl, 10.76; N, 12.65; S, 9.69; Zn, 9.80%. IR (cm^{-1}). NH; 3325, Phenyl NH; 1651, C=O; 1593, C=N. ^1H NMR (DMSO-d_6) δ: 10.23 (s, 1H, NH phenyl), 4.21–4.24 (m, 2H, CH_2), 2.17 (s, 3H, N=C=CH_3), 1.26 (t, 3H, CH_3), Molar conductivity (ohm^{-1} cm^2 mol^{-1}): 21.33. $\mu_{eff.}$ Diamagnetic.

2.1.2.2. $C_{24}H_{26}Cl_2CoN_6O_4S_2$ (CoL_2). Anal. Calc. C, 43.91; H, 3.99; Cl, 10.80; Co, 8.98; N, 12.80; S, 9.77%. Found: C, 43.93; H, 3.97; Cl, 10.80; Co, 9.05; N, 12.77; S, 9.80%. IR (cm^{-1}). 3303, Phenyl NH; 1652, C=O; 1590, C=N. Molar conductivity (ohm^{-1} cm^2 mol^{-1}): 3.78. $\mu_{eff.}$ 4.33 BM.

2.1.2.3. $C_{24}H_{26}Cl_2N_6NiO_4S_2$ (NiL_2). Anal. Calc. C, 43.93; H, 3.99; Cl, 10.81; N, 12.81; Ni, 8.94; S, 9.77%. Found: C, 43.91; H, 4.02; Cl, 10.82; N, 12.79; Ni, 9.01; S, 9.81%. IR (cm^{-1}). 3314, Phenyl NH; 1654, C=O; 1590, C=N. Molar conductivity (ohm^{-1} cm^2 mol^{-1}): 6.93. $\mu_{eff.}$ 3.12 BM.

2.1.2.4. $C_{12}H_{19}Cl_2CuN_3O_5S$ (CuL). Anal. Calc. C, 31.90; H, 4.24; Cl, 15.69; Cu, 14.06; N, 9.30; S, 7.10%. Found: C, 31.96; H, 4.26; Cl, 15.74; Cu, 14.01; N, 9.59; S, 7.10%. IR (cm^{-1}). 3310, Phenyl NH; 1639, C=O; 1594, C=N. λ_{max} (nm), 440–460, 670. λ_{max} (nm): 306 and 367. Molar conductivity (ohm^{-1} cm^2 mol^{-1}): 19.78. $\mu_{eff.}$ 1.86 BM.

2.2. Crystal structure analysis of ethyl 2-(2-(4-chlorophenylcarbamothioyl)hydrazono)propanoate [LH]

A selected crystal of LH was mounted on the tip of a 200 μm Mitagen loop with perfluorinated oil and cooled rapidly to 100 K in a stream of cold nitrogen. Data were collected on an Oxford Diffraction, (Agilent Technologies), SuperNova X-ray diffractometer equipped with an Oxford Cryosystems Cobra Low temperature device using Cu Kα radiation (α = 154.178 pm) from a SuperNova Cu X-ray micro source and focusing mirror optics. The structures were solved by direct methods and refined against F^2 by full-matrix least-squares using the program SHELXTL [23]. Full data collection and refinement details are given in Table 1.

2.3. Cell lines and culture conditions

Human chronic myelogenous leukemia (K-562) was obtained from Prof. Kondaiah, Indian Institute of Science (Bangalore, India). Colon adenocarcinoma (COLO-205) and non-tumor cell line (VERO, renal, green monkey) was purchased from National Centre for Cell Science (Pune, India). K-562 and COLO-205 cell lines were cultured in RPMI-1640 supplemented with 10% FCS (Invitrogen, USA), penicillin G (100 IU/mL) and streptomycin (100 μg/mL) at 37 °C in a humidified 5% CO2 atmosphere. VERO cell lines were maintained in MEM medium.

2.4. Preparation of working stock

Solutions were freshly prepared by dissolving the prepared compounds in DMSO to a concentration of 50 mM and further diluted with RPMI-1640 for the experiments. Each experiment contained two controls: cell control (untreated cells) and

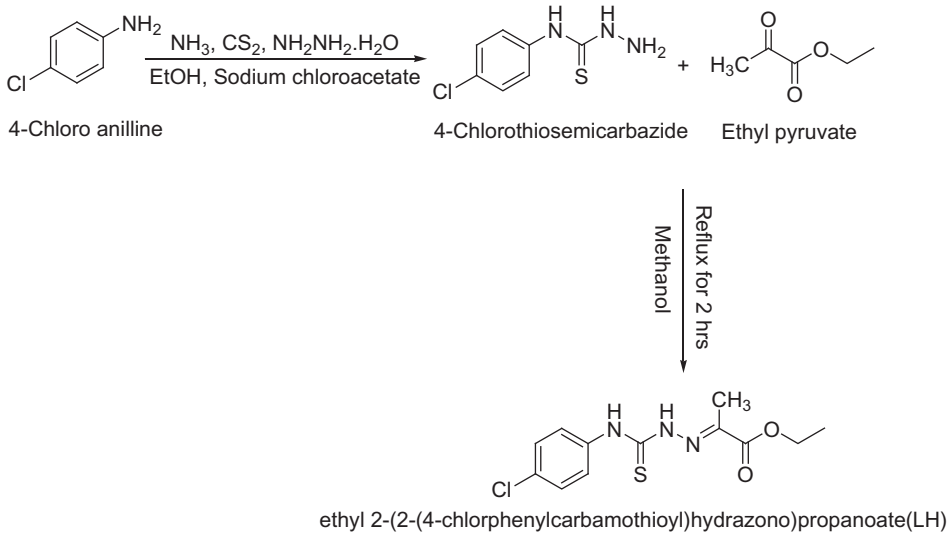

Scheme 1. Synthetic route for the preparation of ligand LH.

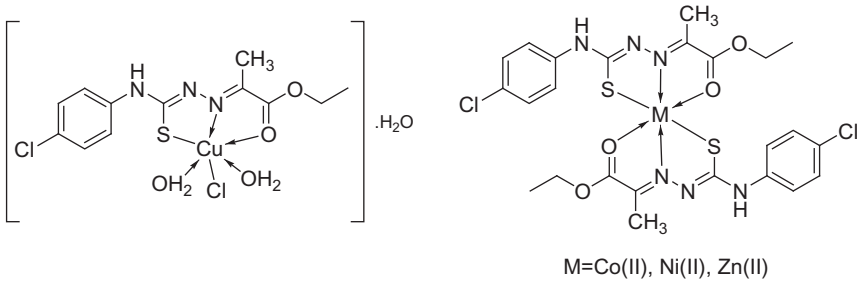

Scheme 2. Proposed structures of the complexes.

Table 1
Crystal data and crystal refinements of LH.

Crystal data	LH
Empirical formula	$C_{12}H_{14}ClN_3O_2S$
Formula mass	299.77
Crystal size (mm)	0.40 × 0.40 × 0.20
Crystal system	monoclinic
Space group	*P*21/*c*
a (pm)	1063.99(4)
b (pm)	1256.02(4)
c (pm)	1073.88(5)
β (°)	106.142(4)
V ($pm^3 \times 10^6$)	1378.55(9)
Z	4
D_{calc} ($g\ cm^{-3}$)	1.444
μ (cm^{-1}) (Mo Kα)	0.430
T (K)	100
$2\theta_{(max)}$ (°)	52.74
Index range	
h	−13 → 9
k	−12 → 15
l	−13 → 12
Reflections collected	6196
Unique reflections (R_{int})	2808
Reflections with $F_o > 4\sigma(F_o)$	2480
Number of parameters	182
R_1	0.0290
wR_2 (all data)	0.0774
Maximum and minimum residual density (($e\ pm^{-3}) \times 10^{-6}$)	0.339, −0.244

additional control (cells treated with maximal concentration of used DMSO solution-less than 0.01%).

2.5. In vitro cytotoxicity evaluation

2.5.1. MTT assay

MTT assay was carried out as described earlier [24,25], with slight modifications. Briefly, exponentially growing cells were seeded at a density of 5×10^4 cells/mL, incubated for 24 h and treated with various concentrations of CoL_2, CuL and NiL_2 (0.5–250 μM). After 48 h of incubation, MTT reagent (1 mg/mL) was added and incubated for 4 h. Formazan crystals formed were dissolved by adding 100 μL of DMSO and absorbance were measured at 570 nm using microplate reader (Bio-Rad, USA). A graph of concentration versus percentage cell viability was plotted and IC_{50} values were calculated.

2.5.2. LDH release assay

Release of lactate dehydrogenase (LDH) is an indicator of loss of membrane integrity and hence cell injury. This assay was designed to estimate the number of nonviable cells present in a mixed population of living and dead cells, using standard protocols [26]. 5×10^4 cells/mL were seeded and treated with 20 μM of copper complex (CuL) for 24, 48 and 72 h. The percentage of LDH released upon treatment was analyzed. The percentage of LDH released was calculated as: (LDH activity in media) = (LDH activity in media + intracellular LDH activity) × 100.

2.6. Measurement of mitochondrial membrane potential ($\Delta\Psi m$) and intracellular ROS

The effect of CuL treatment on mitochondrial membrane potential was measured using JC-1 dye (Molecular Probes, USA) as per standard protocol [27]. Cellular ROS levels were evaluated with the redox sensitive dye CM-H2DCFDA (Molecular Probes, USA). For both the experiments, 5×10^4 cells/mL were treated with 15 μM concentration of CuL and incubated for different time periods at 37 °C. After respective treatment period, cells were washed and labeled for 10 min with dye at 37 °C. Cells were then washed, resuspended in PBS, and fluorescence were measured using fluorescence spectrophotometer (Varian, The Netherlands) [27]. JC-1 was excited at 490 nm, and emission was monitored at 530 and 590 nm. CM-H2DCFDA fluorescence emission was measured at 530 nm by exciting at 490 nm.

2.7. Measurement of caspase-3 activity

The activity of caspase-3 in cell lysates was performed using caspase-3 colorimetric assay kit (Sigma, USA), following the manufacturer instructions. 1×10^6 cells/mL were treated with CuL (5 μM) for 48 h and washed with PBS. Thereafter, pellet was suspended in lysis buffer and incubated on ice for 15 min, followed by centrifugation at 20000*g* for 15 min at 4 °C. The supernatant was collected and samples were mixed with assay buffer with or without caspase-3 inhibitor (Ac-DEVD-CHO). Finally, caspase-3 substrate (Ac-DEVD-pNA) was added to all the samples and incubated at 37 °C for 90 min. Absorbance was recorded at 405 nm. Units of caspase-3 were determined from a standard curve.

2.8. DNA fragmentation assay

The DNA fragmentation assay was performed as described previously with slight modifications [28]. 5×10^5 cells per well were cultured for 48 h with 5 and 25 μM of CuL. The cells were washed twice with PBS (4 °C, pH 7.4) and collected by centrifugation at 250*g* for 5 min. The pellet was then treated with 0.5 mL of lysis buffer (1 M Tris–HCl, pH 7.4, 0.5 M EDTA, 10% sucrose) for overnight at room temperature. Supernatants were collected, treated with 20% SDS and 100 μg/mL RNase, and incubated at 56 °C for 8 h. After incubation, Proteinase K was added and further incubated over night at 56 °C. DNA was precipitated using 10 M ammonium acetate and absolute alcohol, stored at −80 °C over night, and washed with 70% ethanol at 13000 rpm. DNA was then collected and dissolved in TE buffer (10 mM Tris pH 8.0, EDTA 1 mM). Purity of extracted DNA was checked by performing diphenylamine method. For analysis, 10–20 μL of DNA was loaded on a 1.5% agarose gel containing 10 mg/mL ethidium bromide. Electrophoresis was performed in 0.5× Tris borate–EDTA buffer (pH 8.0) at 100 V for 1 h, and fragmented DNA was visualized and photographed using gel documentation system (DNR, Israel).

2.9. Acridine orange–ethidium bromide (AO/EB) double staining

The morphological changes in COLO-205 cells upon treatment with CuL due to apoptosis were detected by performing fluorescence microscopy using acridine orange (AO) and ethidium bromide (EB) staining [29]. Briefly, 1×10^4 cells/mL were seeded on to cover slip, and treated with CuL for 48 h. After treatment, cells were washed with PBS and stained with AO/EB (working concentration of 10 μg/mL) dye for 10 min. The cells were then washed twice with PBS, mounted and immediately observed under fluorescence microscope (Olympus, Japan) using blue filter.

2.10. Cell cycle analysis

Cells were cultured and treated with the different concentration of CuL (5, 10, and 20 μM). After 48 h of treatment, cells were harvested, washed and fixed at 4 °C in 70% ethanol overnight. Fixed cells were washed and incubated at 37 °C with RNase (20 mg/mL) for 4 to 5 h. After RNase treatment, propidium iodide (PI, 1 mg/mL) was added and incubated in dark at room temperature for 30 min before acquiring the flow cytometric reading (FACS calibur using Cell Quest Pro software, BD Biosciences, USA). The percentage of cells in sub-G_0/G_1, G_0/G_1, S and G_2/M phase were determined. At least 10000 cells were sorted per FACS experiment.

2.11. Qualitative assessment of apoptosis by performing confocal imaging

Annexin V/PI labeling assay was performed as per the manufacturer instructions (Invitrogen, USA). Briefly, 1×10^6 cells were treated with CuL (20 μM) for 48 h, washed with ice cold PBS and resuspended in binding buffer. Then the cells were stained with annexin V conjugated to FITC (25 μg/mL) and PI (100 μg/mL) for 15 min in dark. Subsequently, cells were washed and resuspended in annexin V binding buffer, spread over a slide and observed under an inverted confocal laser scanning microscope (LSM 510 META; Zeiss). Imaging was performed to visualize the early and late apoptotic cells.

2.12. Statistical analysis

All the results have been expressed as the mean ± S.E. for data obtained from at least three separate experiments. Data were analyzed for statistical significance by the paired *t* test and $p < 0.05$ values were considered to indicate statistically significant differences.

3. Results and discussion

3.1. Molar conductivity measurements

Molar conductance values of complexes in DMSO at concentration 10^{-3} M fall in the range 1.29–21.33 mho cm^2 mol^{-1}. These values are much less than that expected for 1:1 electrolytes (65–90 mho cm^2 mol^{-1}) and hence are non-electrolytic in nature [30]. The analytical and physicochemical data of the complexes are summarized in experimental section.

3.2. IR spectral studies

Comparison of the IR spectra of the metal complexes with that of the free ligand revealed the tridentate behavior of the ligand coordinating through >C═O, >C═N and >C═S groups. As there are two five-membered coordination rings adjacent to each other, it would impose considerable strain. The negative shift of ν(>C═O) and ν(>C═N) bonds of the ligand on coordination suggests its association with metal ions through carbonyl oxygen and azomethine nitrogen. The bands observed for free LH at 3290 and 3249 cm^{-1} may be assigned to the symmetric vibrations of the ν(NH). The absence of a band at 2500 cm^{-1} indicates the thioketo nature of free LH in the solid state [31]. The ν(>C═S) band, observed at 752 cm^{-1} in the spectrum of the free LH, shifts by 60 ± 67 cm^{-1} to lower wave numbers in the complexes as a result of enolization and consequent coordination to the metal through the deprotonated thiolate [21]. This is also supported by the disappearance of the band at 3249 cm^{-1} assigned to ν(NH) in the spectrum of ligand. Thus the ligand apparently coordinates through the N, O and S atoms.

3.3. NMR spectral studies

The ligand LH displays two sharp singlets at 11.01 and 10.00 ppm attributed to the thiohydrazinic and phenyl NH, respectively. The first signal disappeared on complexation with Zn(II) ion, indicating the thioenolisation and subsequent coordination of sulfur via deprotonation. Further no peak corresponding to ═SH was observed in the spectrum indicating the sulfur coordination through deprotonation. The aromatic protons observed in the region 7.44–7.64 ppm show small shifts on coordination, due to variation in electron density and steric constraints brought about by chelation. A multiplet at 4.21 and a triplet at 1.26 ppm are assigned to CH_2 and CH_3 protons of ester, respectively. The CH_3 proton signal observed at 2.17 ppm in ligand shifts downfield due to the involvement of the adjacent nitrogen of azomethine group >C═N in bonding with the Zn(II) ion, as a result of which the CH_3 protons become less shielded.

^{13}C NMR spectrum of ligand show a signal at 177.71 ppm corresponds to the thioamide carbon (HN═C═S). The resonances at 164.14 and 140.07 are assigned to >C═N and >C═O, respectively, the methylene and methyl carbon signals of ester group are observed at 61.25 and 14.02, respectively. The ^{13}C NMR spectrum of Zn(II) complex showed a downfield shift of signal corresponding to carbonyl, azomethine and thioamide carbon suggesting the coordination through carbonyl oxygen, azomethine nitrogen and thioamide sulfur.

3.4. Mass spectral studies

The mass spectrum of the ligand shows a molecular ion peak m/z at 299 (M^+) corresponds to the molecular weight of the ligand and some prominent signals corresponding to its various fragments and isotopes.

3.5. Magnetic properties, electronic and EPR spectral studies

The electronic spectrum of ligands show bands around 276, 310 and 360 nm. The first band ~276 nm is assigned to a ligand $\pi \rightarrow \pi^*$ transition, while the band around 300–310 nm to $n \rightarrow \pi^*$ transition associated with imine function of thiosemicarbazone. This band shifts to lower energies upon complexation. Another band observed at 330–360 nm region is assigned to $n \rightarrow \pi^*$ transition originating from the thioamide function of thiosemicarbazone [32].

The UV–Vis spectrum of Cu(II) complex exhibits bands around 455 nm and 670 nm attributable to C.T. transition of S → Cu(II) [33] and the d–d transition, $^2E \rightarrow {}^2T_2$, respectively, corresponding to octahedral structure [33]. The magnetic moment of 1.86 BM for Cu(II) supports octahedral structure for the complex [34]. The broad isotropic peak observed with g_{iso} 2.01 and 2.03 in the X-band EPR spectra at RT and LNT suggest the absence of spin–spin interaction in the complex [21]. In the electronic spectrum of nickel complex, three d–d bands were observed at 913, 617, and 371 nm attributable to spin-allowed transitions $^3A_{2g} \rightarrow {}^3T_{2g}$, $^3A_{2g} \rightarrow {}^3T_{1g}$ and $^3A_{2g} \rightarrow {}^3T_{1g}$ (P) respectively, representing octahedral geometry for the complex [35]; the magnetic moment 3.12 BM obtained for the complex suggest the same [33]. The electronic spectrum of Co(II) complex shows absorption at ~370 nm and is assigned to LMCT transition [36]. The peaks around 438–450 and 640–670 nm were attributed to $^4T_{1g}(F) \rightarrow {}^4T_{1g}$ (P) and $^4T_{1g} \rightarrow {}^4A_{2g}$ assigning an octahedral structure for the complex with the magnetic moment value 4.33 BM [21,37]. The diamagnetic zinc complexes show absorptions only in the higher frequency region with high extinction coefficient values attributed to the ligand electron transitions.

3.6. Electrochemical studies

The redox activity of ligand and its complexes were studied in the range +0.2 to −0.8 V versus the ferrocene–ferrocenium redox system in DMSO (0.1 M tetrabutylammonium bromide supporting electrolyte). No peak corresponding to the reduction has been observed down to −0.8 V, as the ligand is shown to be electrochemically inactive in the potential range studied. Further the nickel, cobalt and zinc complexes were also found to be electrochemically inactive. The analysis of cyclic voltammetric responses of copper complex with the scan rate varying from 0.05 to 0.15 vs^{-1} gives the evidence for a quasi-reversible one electron redox process. At a scan rate of 0.05 vs^{-1}, the copper complex exhibits a pair of cathodic and anodic peak potentials at −0.043 V and +0.305 V, respectively, representing the Cu(II)/Cu(I) couple. The negative shift of ΔEp > 59 mV (ΔEp is the difference in the anodic and cathodic peak potentials) and Epc (cathodic peak potential) with increasing scan rate suggest a quasi-reversible nature of the system [38].

3.7. Thermal studies

Thermogravimetric analysis of the complexes has been carried out in nitrogen atmosphere with a heating rate of 10 °C/min. The thermogram of $[CuLCl(H_2O)_2]^*H_2O$ complex exhibits several thermal events. The first weight loss of 3.81% (cal 3.98%) in the temperature range of 60–100 °C corresponds to the loss of a lattice water molecule. The second weight loss of 8.12% (cal 7.96%) in 160–230 °C corresponds to two coordinated water molecules. The corresponding DTA peak at 190 °C in the complex signifies the endothermic process. Further decomposition of 74.81% (73.70%) above 250 °C corresponds to the combined loss of coordinated chloride and the ligand. Whereas the thermograms of Co(II) and Ni(II) shows no weight loss in the region 30–200 °C indicating the absence of lattice or coordinated water molecules. Weight loss of 87.4% and 89.16%, in the temperature range 200–400 °C, is due to the loss of ligand in the respective metal complexes. The plateau obtained above 700 °C corresponds to the formation of stable respective metal oxides.

3.8. Crystallographic studies of LH

The ligand LH (CCDC 978614) crystallized as yellow colored crystals in monoclinic crystal system having space group $C2/c$ with $a = 10.639$ Å, $b = 12.5602$ Å, $c = 10.7388$ Å, $\alpha = \gamma = 90.00°$, $\beta = 106.142°$, $V = 1378.55$ Å^3 and $Z = 4.00$. Details of the data collection and refinements are given in Table 1. Selected bond lengths, bond angles and torsion angles are given in Tables 2–4, respectively. The ORTEP diagram is shown in Fig. 1.

The bond angles around C8, viz. N3–C8–C9 = 117.31(13)°, N3–C8–C10 = 123.38(13)°, C9–C8–C10 = 119.31(13)° clearly reveals the sp^2 hybridized state of C8. The bond angles around N2 viz., N3–N2–C7 = 120.10(13)°, N3–N2–H2B = 119.3(13)°, and C7–N2–

Table 2
Selected bond lengths (Å) of LH.

Atoms	Bond distances (Å)	Atoms	Bond distances (Å)
Cl1–C4	1.7414(15)	C8–C9	1.498(2)
S1–C7	1.6720(15)	C8–C10	1.500(2)
O1–C10	1.2182(18)	C9–H9A	0.9800
N1–C7	1.3440(19)	C9–H9B	0.9800
N1–C1	1.4157(18)	C11–C12	1.506(2)
N2–N3	1.3629(17)	C11–H11A	0.9900
N3–C8	1.2893(19)	C12–H12A	0.9800
C1–C6	1.390(2)	C12–H12B	0.9800
C1–C2	1.395(2)	C12–H12C	0.9800

Table 3
Selected bond angles of LH (°).

Atoms	Bond angles (°)	Atoms	Bond angles (°)
C10–O2–C11	115.86(11)	C2–C1–N1	116.18(13)
C7–N1–C1	130.32(13)	C3–C2–C1	120.46(14)
C7–N1–H1A	113.5(13)	O1–C10–O2	124.25(14)
C1–N1–H1A	116.0(13)	O1–C10–C8	124.24(13)
N3–N2–C7	120.10(13)	O2–C11–H11A	110.3
C7–N2–H2B	120.6(13)	O2–C11–H11B	110.3
C8–N3–N2	120.22(13)	N1–C7–S1	127.51(12)
C6–C1–C2	119.83(13)	O2–C11–C12	106.93(12)
C6–C1–N1	123.94(13)	N2–C7–S1	118.00(11)

H2B = 120.6(13)° also illustrate the sp^2 hybridized state of N2. The bond distance of 1.3629(17) Å, 1.3687(19) Å confirms the single bond character of the N2–N3 and N2–C7 linkage. The C–C bond distances and C–C–C bond angles of phenyl ring are in accordance with the values reported in literature [21,39,40]. The bond distances C=O (C2=O1=1.231 Å) and C=N (C8=N3=1.2893(19) Å) are in conformity with the double bond character. The torsional angle −178.25(13)° exhibited by N3–C8–C10–O2 and 2.0(2)° by N3–C8–C10–O1 indicates that N3 and O2 atom are *trans* to one another and N3 and O1 are cis to each other. The torsional angle for N3–N2–C7–S1 = 174.31(10)° clearly shows that S1 and N3 are *trans* to each other. The molecular packing diagram shows two layers of molecules. In each molecule, presence of intra molecular hydrogen bonding stabilizes the crystal packing. The two strong intramolecular hydrogen bonds between N1H and N3 [N1–H...N3 = 2.171(18) Å] and N2H and O1 [N2–H2B...O1 = 1.97(2) Å] are also present. It gives a significant contribution to the planarity of the thiosemicarbazide moiety.

3.9. Evaluation of cytotoxicity and possible mechanism of cell death

To evaluate the role of synthesised metal complexes (CoL_2, NiL_2 and CuL) as antiproliferative agents, they were tested on two different human cell lines, K-562 and COLO-205. Both the cells were treated with different concentrations of CoL_2, NiL_2 and CuL for 48 h and subjected to MTT assay, with cisplatin as a positive control [39]. All tested complexes showed noticeable antiproliferative effect (Fig. 2a) and IC_{50} values (Table 5). Among the panel of complexes, CuL exhibited strong dose dependent antiproliferative activity against COLO-205 cell line (IC_{50} value 8.65 μM) comparable with positive control cisplatin (IC_{50} value of 7.24 μM), than against more resistant [41] cell line K-562 (IC_{50} of 15.16 μM). On the other hand, cobalt (CoL_2) and nickel (NiL_2) complexes exerted weak activity against K-562 ($IC_{50} > 250$) and showed comparatively more activity against COLO-205. As copper complex (CuL) showed higher antiproliferative activity among all tested complexes, CuL is selected further for mechanistic studies. Further, it is noticed that ethyl pyruvate derived thiosemicarbazone ligand coordinated with copper ion has a synergetic effect on the antitumor activity compared to ligand alone (Table 5). Also copper alone did not induced any significant cytotoxicity on the cell lines tested. The enhanced activity of copper complex is mainly attributed to redox active metal ion and the ligand attached. Interestingly, cytotoxicity of these molecules on a non tumor cell line (VERO cell line) showed IC_{50} value higher than 250 μM, which might suggest these compounds have a low toxicity to normal cells.

LDH is a cytoplasmic enzyme that is constantly expressed in all cells, enables its use in assessing plasma membrane integrity by determining the amount of LDH in extracellular space [40]. LDH release assay was performed as a means of cytotoxicity in terms of cellular damage on CuL treated COLO-205 cells. A significant ($p < 0.01$) time dependent increase in the release of LDH into the surrounding media was noticed upon treatment with CuL (20 μM) compared to control (Fig. 2b). This may be due to intense cellular damage caused by CuL complex upon treatment. Results from LDH assay are consistent with cytotoxic MTT assay results and confirm the potential cytotoxic effect of CuL complex.

Table 4
Torsional angles of LH.

Atoms	Bond angles (°)	Atoms	Bond angles (°)
C1–N1–C7–N2	178.06(13)	C7–N2–N3–C8	178.71(13)
C1–N1–C7–S1	−0.8(2)	C7–N1–C1–C6	24.2(2)
N3–N2–C7–N1	−4.69(19)	C7–N1–C1–C2	−158.36(15)
N3–N2–C7–S1	174.31(10)	C6–C1–C2–C3	−1.4(2)
N3–C8–C10–O2	−178.25(13)	N1–C1–C2–C3	−178.93(13)
C9A–C8–C10–O1	2.0(2)	Cl1–C4–C5–C6	179.74(11)
C2–C3–C4–F1	178.51(12)	C3–C4–C5–C6	−0.8(2)

3.10. Copper complex alters $\Delta\Psi_m$ without generating ROS

To supplement the encouraging cytotoxicity results of CuL, it was thought to explicate its molecular basis. The changes in the $\Delta\Psi_m$ after treating COLO-205 cells with 15 μM of CuL were measured. A time dependent significant ($p < 0.01$) fall in the membrane potential was observed from 6 h of treatment and continued as time increased (Fig. 2c). Pre-incubation with 50 μM N-acetyl cysteine (NAC) did not reversed the fall in $\Delta\Psi_m$.

To elucidate the possible pathway involved in the copper complex induced cell death, ROS levels were monitored at different time points by treating COLO-205 cells with 15 μM CuL. However, significant increase in the ROS level was not observed in CuL treated cells compared to control cells (Fig. 2d). Cells pretreated with NAC also did not show any changes in ROS level. Hence, comparing the close correspondence between the $\Delta\Psi_m$ fall and absence of ROS in CuL treated cells, one can rule out the involvement of ROS in altering the $\Delta\Psi_m$. Since fall in $\Delta\Psi_m$ has direct relationship with caspase mediated cell death [42], it was proved that mitochondrion plays an important role in the cell death process. This result further confirms the potential of CuL to destroy integrity of mitochondrial membrane.

3.11. Measurement of caspase-3 activity and DNA fragmentation

To check whether CuL induced cell death is mediated by apoptosis; caspase-3 activity and DNA fragmentation assay were performed. CuL induced apoptosis was first demonstrated by caspase-3 activity assay. Changes in the caspase-3 activity upon treatment (5 μM) of CuL in COLO-205 cells were measured using colorimetric assay kit. A significant ($p < 0.01$) time dependent increase in the caspase-3 activity was observed upon treatment, confirming the apoptotic mode of cell death (Fig. 2e). Activation of caspase-3 often leads to the activation of caspase activated DNase (ICAD) through removal of its inhibitor site, inhibitor of caspase activated DNase (ICAD) [43] thereby playing important role in the CAD dependent induction of apoptosis [44]. Such activated CAD cleaves the DNA at internucleosomal region and leads to DNA fragmentation in apoptotic cell. Therefore, we analyzed the DNA fragmentation in cells upon CuL treatment. In our studies, COLO-205 cells treated for 48 h with 5 and 25 μM CuL showed typical DNA ladder conformation upon gel electrophoresis (Fig. 2f), which is the major biochemical hallmark of apoptosis. A notable increase in the percent DNA damage was observed with increasing concentrations of CuL, with control cells showing no laddering of DNA.

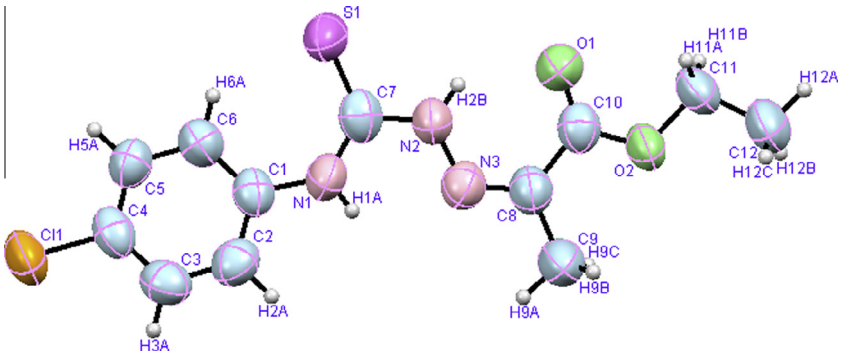

Fig. 1. ORTEP diagram of LH.

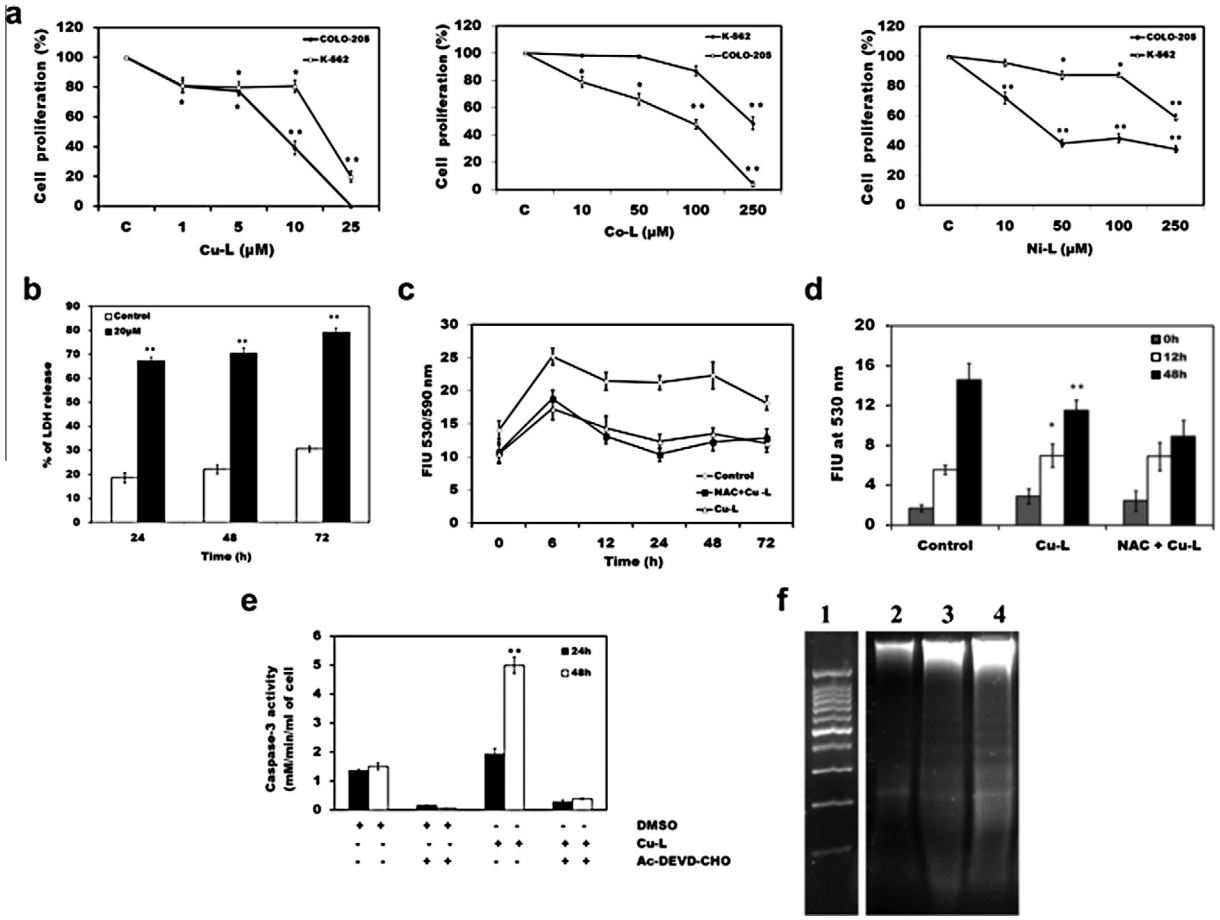

Fig. 2. Effects of metal complexes of ethyl 2-(2-(4-chlorophenylcarbamothioyl)hydrazono)propanoate on cancer cell lines. (a) Cytotoxic effect of test complexes on K-562 and COLO-205 cell lines after 48 h treatment was assessed by performing MTT assay. (b) LDH release was assayed after treating COLO-205 cells with 20 μM of CuL for 24, 48 & 72 h treatment. (c) Time-dependent measurement of $\Delta\Psi_m$ upon 15 μM CuL treatment on COLO-205 cells with or without 30 min pre-incubation with 50 μM NAC was measured using JC-1 dye. (d) Intracellular ROS level was measured using CM-H_2DCFDA. COLO-205 cells were treated with 15 μM CuL with or without pre-treatment of NAC for 30 min and were stained and fluorescence was measured. (e) Caspase-3 activity was determined in COLO-205 cells treated with 5 μM of CuL for 24 and 48 h, using DEVD-pNA as substrate at 405 nm. Activity was measured in terms of concentration of pNA formed per min per ml of cell lysate. (f) CuL induces internucleosomal DNA fragmentation. DNA separated from COLO-205 cells treated for 48 h with 5 and 25 μM CuL, were subjected to electrophoresis in 1.5% agarose. *Lane 1*, 200 bp DNA ladder; *Lane 2*, DMSO control; *Lane 3*, 5 μM CuL; *Lane 4*, 25 μM CuL. Data presented are representative of two experiments and the results were same. The data represents Mean ± SE ($n = 3$). $^{*}p < 0.05$, $^{**}p < 0.01$ compared with the control group.

3.12. Morphological evaluation of apoptosis

3.12.1. Acridine orange–ethidium bromide (AO/EB) double staining

Nuclear morphology of cells undergoing apoptosis was phenotypically evidenced by staining the cells with AO/EB. COLO-205 cells treated for 48 h with 15 μM of CuL were stained and observed under fluorescent microscope (Fig. 3). Cells treated with DMSO stained green, represent viable cells with intact membrane. In contrast, CuL treated cells exhibited apoptotic morphological changes including condensed chromatin and fragmented nuclei. A stronger apoptosis signal was observed with treatment of the CuL, strongly suggesting the apoptotic mode of cell death, since chromatin condensation, loss of membrane integrity, formation of apoptotic bodies and formation of membrane blebbing are the major events involved in apoptotic mode of cell death [45].

Table 5
In vitro antiproliferative activity of the complexes evaluated in human cancer cell lines after 48 h exposure. Results are mean of three independent experiments.

Complexes	IC_{50} (μM)		VERO
	COLO-205	K-562	
Cu-L	8.65	15.16	120.15
Co-L_2	99.94	>250.00	>250.00
Ni-L_2	94.75	>250.00	>250.00
LH	230.00	>250.00	>250.00
Cisplatin	7.87	5.99	ND

ND – Not determined.

3.12.2. Cell cycle analysis and annexin V-FITC/PI staining

To further support our findings, we checked the effect of CuL complex on cell cycle progression by flow cytometry. COLO-205 cells incubated with different concentrations of CuL for 48 h showed significant sub-G_0/G_1 peaks indicating apoptosis, and the percentage of apoptotic cells presented a dose-dependent increase from 5 to 20 μM (sub G_0/G_1: 4.98–20.64%) compared to control (Fig. 4a–d). The histograms of CuL treated cells did not show any significant change in cell cycle profile, except sub G_0/G_1 population, suggesting the inefficiency of the complex to induce cell cycle arrest at any phase of the cell cycle. Put together, cell cycle analysis data clearly indicate that the mechanism of cytotoxicity

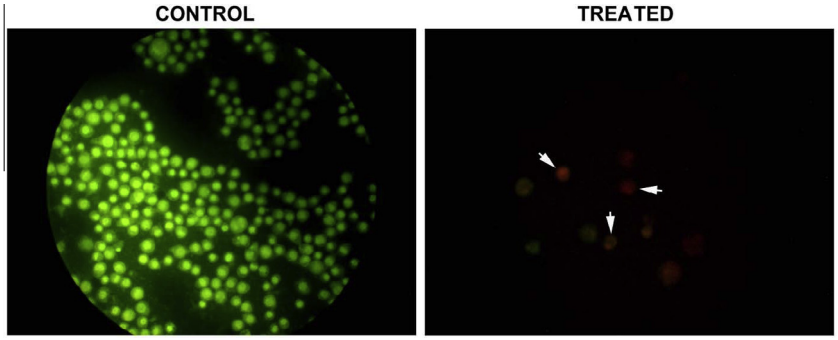

Fig. 3. Detection of apoptosis by fluorescence microscopy. Acridine orange–ethidium bromide double staining. Morphological evidence of apoptosis was obtained by performing AO/EB double staining. COLO-205 cells were treated with 15 μM of CuL for 48 h and fluorescence microscopic imaging was done. Arrow heads indicate cellular shrinkage and nuclear granulation.

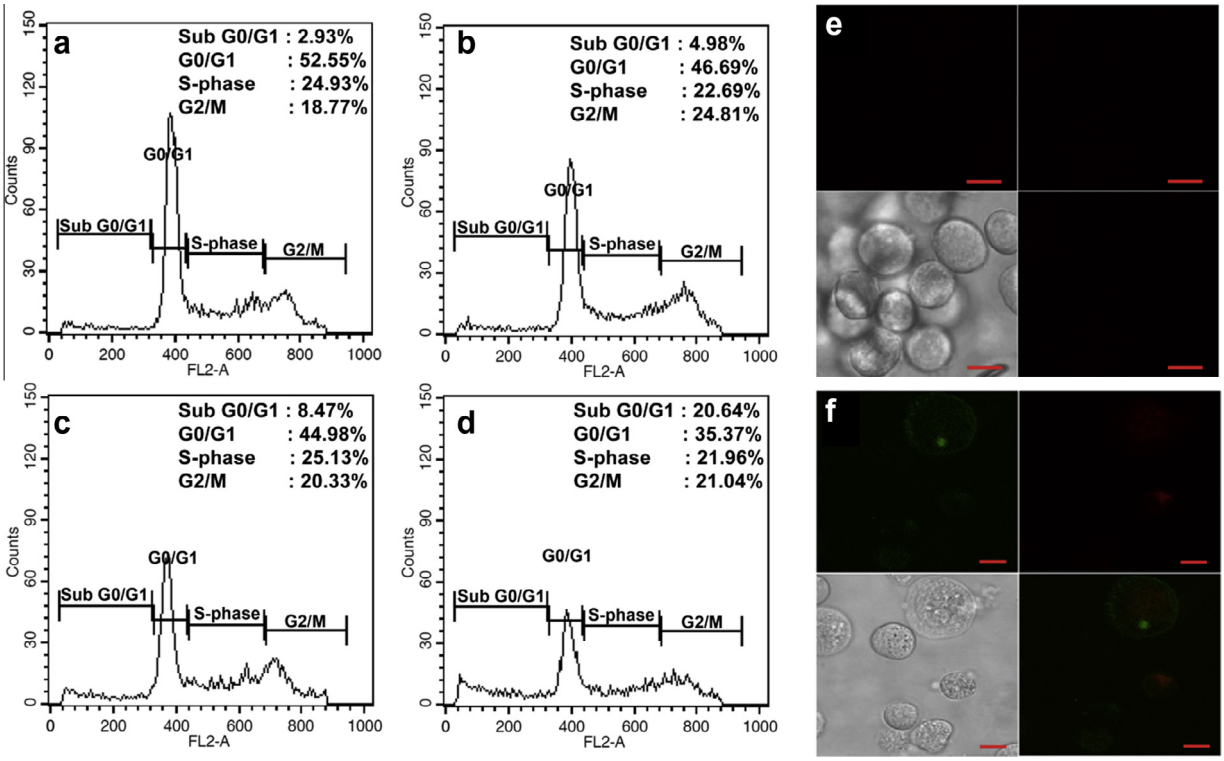

Fig. 4. Flow cytometric determination of effect of metal complexes on cell cycle and apoptosis. (a–d) Impact of CuL on cell cycle of COLO-205 cells after the treatment for 48 h. Cell cycle distribution was analyzed by flow cytometry. Histograms are representative of three independent experiments. (e, f) Confocal micrographs of CuL treated COLO-205 cells, stained with Annexin V/PI. (e) Cells treated with DMSO. (f) Cells treated with CuL showing both Annexin V/PI and Annexin V (late and early of stage apoptosis) positive cells.

by CuL may primarily involve apoptotic mode of cell death induction.

These conclusions were furthermore verified by observing the annexin V-FITC/PI stained cells under a confocal microscope. After 48 h of treatment with CuL, most of the control cells were negative for both annexin V-FITC and PI (Fig. 4e). Upon CuL treatment, cells were stained with either annexin V-FITC (green color) alone or by both annexin V-FITC (green color) and PI (red color), suggesting presence of both early apoptotic and late apoptotic cells with complete membrane damage (Fig. 4f). These results clearly suggest that apoptosis could be the mechanism of cell death induced by the CuL.

4. Conclusion

The ligand LH acts as tridentate monobasic chelate with N, O and S as the donating sites toward Co(II), Ni(II), Cu(II) and Zn(II) ions leading to octahedral geometries. Antiproliferative activity of panel of complexes synthesized was evaluated. Among the complexes tested, CuL showed potent antiproliferative activity with its activity comparable to that of standard drug, cisplatin. The CuL antiproliferative effect was mainly exerted through the induction of apoptotic cell death as confirmed by flow cytometric sub G_0/G_1 cells accumulation and confocal imaging. Possible mechanism of cell death induction was through caspase dependent intrinsic mitochondrial mediated apoptotic pathway.

Presence of greater number of nucleophilic sites (H_2O) seems to have a greater influence on the overall biological activity of the complex. The biological activity has been augmented specifically by redox active Cu and presence of water.

Acknowledgments

The authors thank the USIC, Karnatak University, Dharwad for providing the spectral facilities. Recording ^{1}H and ^{13}C Spectral studies (MU London) and ESR spectra (IIT Bombay) are gratefully acknowledged. Dr. Aishakhanam H. Pathan is thankful to University Grants Commission (India) for providing Research fellowship in Science for Meritorious Students. Miss Asha K. Ramesh is thankful to Indian Council of Medical Research (India) for financial support. Authors also thank Prof. Kondaiah P, Indian Institute of Science and C-CAMP, NCBS, Bangalore for providing FACS facility. Authors also thank Prof. M.V. Kulkarni for language corrections. Dr. K.B. Gudasi is thankful to the Association of Commonwealth Universities (United Kingdom), for Commonwealth fellowship.

Appendix A. Supplementary material

CCDC 978614 contains the supplementary crystallographic data for LH. These data can be obtained free of charge from The Cambridge Crystallographic Data Centre via www.ccdc.cam.ac.uk/data_request/cif. Supplementary data associated with this article can be found, in the online version, at http://dx.doi.org/10.1016/j.ica.2015.03.013.

References

[1] C. Deegan, B. Coyle, M. McCann, M. Devereux, D. Egan, Chem. Biol. Interact. 164 (2006) 115.
[2] Z. Afrasiabi, E. Sinn, J. Chen, Y. Ma, A.L. Rheingold, L.N. Zakharov, N. Rath, S. Padhye, Inorg. Chim. Acta 357 (2004) 271.
[3] R.A. Alderden, M.D. Hall, T.W. Hambley, J. Chem. Educ. 83 (2006) 728.
[4] P.N. Yadav, M.A. Demertzis, D. Kovala-Demertzi, S. Skoulika, D.X. West, Inorg. Chim. Acta 349 (2003) 30.
[5] E. Wong, C.M. Giandomenico, Chem. Rev. 99 (1999) 2451.
[6] T.W. Hambley, Coord. Chem. Rev. 166 (1997) 181.
[7] B. Stordal, N. Pavlakis, R. Davey, Cancer Treat. Rev. 33 (2007) 688.
[8] I. Gojo, M.L. Tidwell, J. Greer, N. Takebe, K. Seiter, M.F. Pochron, B. Johnson, M. Sznol, J.E. Karp, Leuk. Res. 31 (2007) 1165.
[9] A.G. Quiroga, J.M. Perez, I. Lopez-Solera, E.I. Montero, J.R. Masaguer, C. Alonso, C.N. Ranninger, J. Inorg. Biochem. 69 (1998) 275.
[10] A.M. Fialho, A.M. Chakrabarty, Recent Pat. Anticancer Drug Discov. 2 (2007) 224.
[11] A. Diaz, R. Cao, A. Garcia, Monatsh. Chem. 125 (1994) 825.
[12] K. Grancharov, G.J. Krauss, N. Spassovska, J. Miersch, L. Maneva, J. Mladenova, E. Golovinsky, Pharmazie 40 (1985) 574.
[13] S. Chandra, K.K. Sharma, Transition Met. Chem. 9 (1984) 1.
[14] S. Hayami, K. Hashiguchi, K. Inoue, Y. Maedaa, J. Nucl. Radiochem. Sci. 5 (2004) N1.
[15] D.K. Chand, H.J. Schneider, J.A. Aguilar, F. Escarti, E. Garcia-Esspara, S.V. Luis, Inorg. Chim. Acta 316 (2001) 71.
[16] F.L. Lee, E.J. Gabe, L.E. Khoo, W.H. Leong, G. Eng, F.E. Smith, Inorg. Chim. Acta 166 (1989) 257.
[17] L. Savini, P. Massarelli, L. Chiasserini, C. Nencini, C. Pellerano, Farmaco 52 (1997) 609.
[18] H. Kappus, Biochem. Pharmacol. 35 (1986) 1174.
[19] T.W. Gant, D.N.R. Rao, R.P. Mason, G.M. Cohen, Chem. Biol. Interact. 65 (1988) 157.
[20] M.A. Cater, H.B. Pearson, K. Wolyniec, P. Klaver, M. Bilandzic, B.M. Paterson, A.I. Bush, P.O. Humbert, S.L. Fontaine, P.S. Donnelly, Y. Haupt, ACS Chem. Biol. 8 (2013) 1621.
[21] A.H. Pathan, R.P. Bakale, G.N. Naik, C.S. Frampton, K.B. Gudasi, Polyhedron 34 (2012) 149.
[22] S.B. Himara, K.A. Parikh, B.C. Merja, H.H. Parekh, Indian J. Chem., Sect B 42 (2003) 1172.
[23] G.M. Sheldrick, SHELXTL. Version 5.0, Bruker AXS Inc., Madison, Wisconsin, USA, 2001.
[24] T. Mosmann, J. Immunol. Methods 65 (1983) 55.
[25] K.K. Chiruvella, S.K. Sankaran, M. Singh, M. Nambiar, S.C. Raghavan, ICFAI J. Biotechnol. 1 (2007) 7.
[26] C.V. Kavitha, M. Nambiar, Biochem. Pharmacol. 77 (2009) 348.
[27] S. Shenoy, V.S. Vasania, M. Gopal, A. Mehta, Toxicol. Appl. Pharmacol. 222 (2007) 80.
[28] N. Li, K. Ragheb, G. Lawler, J. Sturgis, B. Rajwa, J.A. Melendez, J.P. Robinson, J. Biol. Chem. 278 (2003) 8516.
[29] D. Ribble, N.B. Goldstein, D.A. Norris, Y.G. Shellman, BMC Biotechnol. 5 (2005) 12.
[30] M.A. Affan, F.S. Wan, Z. Ngaini, M. Shamsuddin, Anal. Sci. 13 (2009) 63.
[31] A.H. Pathan, K.B. Gudasi, Med. Chem. Res. 22 (2013) 1504.
[32] Z. Afrasiabi, E. Sinn, S. Padhye, S. Dutta, S. Padhye, C. Newton, C.E. Anson, A.K. Powell, J. Inorg. Biochem. 95 (2003) 306.
[33] H. Okawa, M. Tadokoro, Y. Aratake, M. Ohba, K. Shindo, M. Mitsumi, M. Tomono, D.E. Funton, J. Chem. Soc., Dalton Trans. (1993) 253.
[34] F.A. Cotton, G. Wilkinson, Adv. Inorg. Chem., fifth ed., Wiley, New York, 1988.
[35] J.C. Bailar, H.J. Emeleus, S.R. Nyholm, A.F.T. Dickenson, Comprehensive Inorganic Chemistry, Pergamon, Oxford, UK, 1973.
[36] S. Adsule, V. Barve, D. Chen, F. Ahmed, Q.P. Dou, S. Padhye, F.H. Sarkar, J. Med. Chem. 49 (2006) 7242.
[37] M.B. Ferrari, F. Bisceglie, G. Pelosi, P. Tarasconi, R. Albertini, S. Pinelli, J. Inorg. Biochem. 87 (2001) 137.
[38] J. Wiecek, V. Dokorou, Z. Ciunik, D. Kovala-Demertzi, Polyhedron 28 (2009) 3298.
[39] F.E. Smith, Science 113 (1951) 751.
[40] C. Korzeniewski, D.M. Callewaert, J. Immunol. Methods 64 (1983) 313.
[41] K.K. Palanichamy, N. Sreejayan, A.C. Ontko, J. Inorg. Biochem. 106 (2012) 32.
[42] A. Strasser, L.O. Connor, V.M. Dixit, Annu. Rev. Biochem. 69 (2000) 217.
[43] B.B. Wolf, M. Schuler, F. Echeverri, D.R. Green, J. Biol. Chem. 274 (1999) 30651.
[44] S. Elmore, Toxicol. Pathol. 35 (2007) 495.
[45] P. Mukhopadhyay, M. Rajesh, G. Hasko, B.J. Hawkins, M. Madesh, P. Pacher, Nat. Protoc. 2 (2007) 2295.